Optical phase conjugation in a single-level metallic quantum well

Torsten Andersen and Ole Keller
Institute of Physics, Aalborg University, Pontoppidanstræde 103, DK-9220 Aalborg Øst, Denmark
(Received 11 December 1997; revised manuscript received 11 February 1998)

We present a calculation of the phase conjugated response from a single-level metallic quantum well. The description builds upon a recently developed local-field theory for degenerate four-wave mixing in mesoscopic interaction volumes of condensed media. The single-level quantum well represents the simplest possible configuration of a quantum well phase conjugator. Furthermore, the single-level quantum well is an interesting object, since the optical response contains no dipole terms. The discussion of the response is based on the use of linearly polarized light to excite the process. We demonstrate that the phase conjugation process is extremely efficient in the evanescent regime of the wave-vector spectrum. We also address the problem of plane-wave excitation of the high wave-number end of the evanescent regime. We end our discussion by suggesting the use of a broadband source to excite the process. One such broad angular band source is a quantum wire, and the phase conjugated angular spectrum from a quantum wire is presented and discussed. [S0163-1829(98)01823-2]

I. INTRODUCTION

Studies of the optical properties of quantum wells (single and multiple), surfaces and interfaces have drawn the attention of researchers for two decades, and in recent years, in particular, investigations of the nonlinear electrodynamics have been in focus. Among the many nonlinear phenomena studies of second-harmonic generation,[1–6] sum and difference frequency generation,[4,7] photon drag,[8–11] dc electric-field-induced second-harmonic generation,[12,13] the Kerr effect,[14–17] electronic and vibrational surface Raman scattering,[18–20] two-photon photoemission,[21–25] and generation of higher harmonics[26,27] have played a prominent role.

From a theoretical point of view the description of the above-mentioned structures belongs to the field of mesoscopic electrodynamics. This is so because the interaction length in the direction perpendicular to the plane of the structures is much smaller than the electromagnetic wavelengths in the optical regime. Since the refractive index concept usually is meaningless for structures of only a few monolayers thickness macroscopic approaches have to be abandoned from the outset. Theoretical analyses therefore have to start from the microscopic Maxwell equations combined with the (single-electron) Schrödinger equation.

In the present paper we give a theoretical and numerical description of a nonlinear phenomenon not hitherto studied, to our knowledge, at such interaction lengths, viz. optical phase conjugation by degenerate four-wave mixing in a quantum well structure. Optical phase conjugation is a nonlinear process involving the mutual interaction of four different light waves in a nonlinear medium. If the four waves have the same frequency the process is named degenerate four-wave mixing (DFWM). In the context of solid-state physics one typically starts mixing two counterpropagating beams (called pumps) and a third beam (called the probe) usually not collinear with the pumps. The nonlinear response of the medium (crystal) due to momentum conservation (phase matching) then generates a fourth beam (the phase conjugated signal) propagating oppositely to the probe. Once generated the fourth beam interacts dynamically with the pumps and the probe, thus the name four-wave mixing. In the context of a field quantized description a weak fourth beam is present from the outset due to fluctuations in the vacuum field. Crudely speaking one may say that the phase conjugated field forms a real-time holographic image of the probe field, and this of course points to a number of practical applications of optical phase conjugation. The strength of the degenerate four-wave mixing process depends on the frequency of light in a manner determined by the given nonlinearity of the crystal used. To tailor the frequency response in a controlled manner it would be nice to use a quantum-well system because the frequency dependence of the nonlinearity may be modified and brought to resonance (high efficiency), for instance, by changing the thickness of the well or by using a series of (different) quantum wells, as in a multiple film arrangement.

In a quantum well the (nonlinear) dynamics associated with electron motions parallel and perpendicular to the plane of the well is qualitatively different. Thus, in the direction perpendicular to the plane of the well the electrons may be excited between different subbands, and this can lead to pronounced atomiclike resonance effects. Electron motions parallel to the well plane are associated with intraband transitions in a quasicontinuum of states, and for this kind of excitations the Bloch character of the states is important. If the quantum well is sufficiently thin there is only one bound level (subband), and if this is located below the Fermi energy, the electron dynamics is quasi-two-dimensional. In this work only single-level metallic quantum wells are considered, and for simplicity it is assumed that the electron dynamics parallel to the well plane is free-electron like. In order for a metallic quantum well to have only a single bound level its thickness must not exceed an (a few) atomic monolayer(s). The phase conjugator we deal with in this paper therefore is essentially two-dimensional, and this in and of itself makes an analysis worthwhile.

The usual steady-state description of DFWM is a macroscopic description covering the DFWM process in photorefractive media where the interaction length is long, and the description is limited to cover the far field part of the electromagnetic signal. It is usually based on the assumptions that the amplitudes of the fields are slowly varying on the optical wavelength scale [slowly varying envelope (SVE) approximation], and thus also constant across the individual scattering units (atoms, molecules, etc.). Neglecting the variation of the field across the nonlinear scatterers means that the electric dipole (ED) approximation can be employed. For a comprehensive review of the existing descriptions of optical phase conjugation, as well as of the experimental work, the reader is encouraged to consult Refs. 28–32.

In thin films (quantum wells), however, it is crucial to keep the microscopic dynamics perpendicular to the surface of the phase conjugating mirror when calculating the DFWM response. So far, four-wave mixing in media with two-dimensional translational invariance has only been studied in the context of phase conjugation of surface plasmons[33–35] and of a bulk wave by surface plasmons.[36] In these investigations a macroscopic approach was used.

Especially if one wants to use the DFWM technique to create focusing of phase conjugated dipole radiation with a spatial extent below the classical diffraction limit, where the hitherto appeared descriptions are based on an assumption that the phase conjugator is ideal[37–39] or Kerr like,[40] it is important also to consider the response in the optical near-field region. A Fourier analysis of the field from a radiating mesoscopic object in the coordinates of the plane of the phase conjugator shows a large content of plane-wave components in the near-field regime. Due to the exponentially decaying nature of optical near fields, the length scale under which the substantial part of any optical interaction, linear as well as nonlinear, takes place is of the order of a fraction of the optical wavelength. Considering interaction at such a length scale it is necessary to abandon the otherwise usually adopted SVE and ED approximations.

In the present work we shall present the simplest possible result of using our model for the phase conjugation process. It is achieved using a single quantum well with only one bound state below the Fermi energy. The use of such a single-level quantum well has previously been shown to be feasible to provide a simple description of photon drag in metallic films.[8] The consequence of choosing a single-level quantum well is that the phase conjugated response is limited to be constructed of pure intraband (intersubband) transitions.

Thus, in Sec. II we present the theoretical framework for the present calculations starting from the wave equation for the phase conjugated field, which is calculated using the microscopic Maxwell-Lorentz equations. We discuss the optical phase conjugation response function of an electron in a two-dimensional translational invariant system (e.g., a quantum well), in the form it takes starting from the Liouville equation of motion for the density-matrix operator and the minimal coupling Hamiltonian. The nonlinear response function we derive in the aforementioned manner allows us to calculate the current density induced in the quantum well by the nonlinear mixing of the two pumps and the probe. The radiation from this nonlinear current density is the phase conjugated field. The nonlinear response function deviates from those hitherto established in the sense that it enables us to calculate the spatially rapidly varying microscopic current density on an atomic length scale and not only the spatially averaged (macroscopic) current density. This is essential for quantum-well systems where the well thickness is in the Ångström range. A general theory for DFWM conductivity tensors in mesoscopic interaction volumes we developed and discussed in a previous paper,[41] where also formal aspects of the underlying nonlocal nonlinear electrodynamics were examined. The two-dimensional conservation of momentum is presented and the nonlinear constitutive relation is reduced to its DFWM form. Having established the basic needs to describe the response we set up the self-consistent field equation for the phase conjugated field, and limit our study to the simplest possible configuration, for which the explicit form of the nonlinear conductivity tensors are presented. The consequenses of choosing a probe field with only a single plane-wave Fourier component are analyzed, and the section is finished with a discussion of the infinite barrier (IB) model adopted to describe the quantum well in the numerical work.

With special attention drawn to the optical near field, our numerical work is started in Sec. III with a quantitative discussion of the phase conjugation reflection coefficient from a single-level quantum well, choosing two monolayers of copper as the metallic quantum well. First, we present the reflection coefficient for the phase conjugated light, which includes all components in the Fourier spectrum, propagating as well as evanescent, and then we address the problem of choosing an appropriate relaxation time in a thin quantum well. To excite the whole Fourier spectrum with one plane wave at a time can prove difficult, if not impossible. Instead one might consider the use of a broadband source of one kind or another. To give an impression of how the phase conjugated field looks when excited with a specific broadband source we consider the response when a quantum wire (two-dimensional point dipole) is placed in front of the phase conjugator. Finally, in Sec. IV, we conclude.

II. THEORY

In order to describe nonlinear optical phenomena in mesoscopic media it is in general necessary to abandon macroscopic electrodynamics from the outset,[42,43] and therefore take as a starting point the microscopic Maxwell-Lorentz equations. In these equations the material response at the space-time point $(\vec{r},t)$ is completely characterized by the microscopic current density $\vec{J}(\vec{r},t)$, and the related charge density. In the context of optical phase conjugation it is usually adequate to treat the electrodynamics in the space-frequency domain if the involved light signals are not too short. In the case of DFWM we need only a harmonic analysis at the fundamental frequency ω. By assuming that the electromagnetic field driving the phase conjugated response is of moderate magnitude, it is sufficient to have a knowledge of the linear, $\vec{J}^{(1)}_{-\omega}(\vec{r})$, and the lowest-order nonlinear, $\vec{J}^{(3)}_{-\omega}(\vec{r})$, current-density contributions at the fundamental frequency. With this limitation the wave equation for the phase conjugated (PC) electric field, $\vec{E}_{\mathrm{PC}}(\vec{r};\omega)\equiv\vec{E}_{\mathrm{PC}}(\vec{r})$, takes the form in a DFWM process

$$\left[\overleftrightarrow{\mathbb{I}}\left(\frac{\omega^2}{c_0^2}+\nabla^2\right)-\vec{\nabla}\otimes\vec{\nabla}\right]\cdot\vec{E}_{\mathrm{PC}}(\vec{r}) = -i\mu_0\omega(\vec{J}^{(1)}_{-\omega}(\vec{r})+\vec{J}^{(3)}_{-\omega}(\vec{r})), \tag{1}$$

where $\overleftrightarrow{\mathbb{I}}$ is the (3×3) unit tensor.

A. Microscopic constitutive relations

The microscopic current densities appearing in Eq. (1) may be expressed in terms of the relevant local electric fields through appropriate constitutive relations. Within a single-electron random phase approximation approach it is usually sufficient for a condensed matter system to assume that the induced particle motion is driven by the prevailing (total) electromagnetic field. This means that the linear constitutive relation reads

$$\vec{J}^{(1)}_{-\omega}(\vec{r})=\int\overleftrightarrow{\sigma}(\vec{r},\vec{r}')\cdot\vec{E}_{\mathrm{PC}}(\vec{r}')d^3r', \tag{2}$$

where $\overleftrightarrow{\sigma}(\vec{r},\vec{r}')=\overleftrightarrow{\sigma}(\vec{r},\vec{r}';\omega)$ is the linear and nonlocal single-electron conductivity tensor. The ith element of the first-order current density is thus given by the volume integral of $[\overleftrightarrow{\sigma}\cdot\vec{E}_{\mathrm{PC}}]_i=\Sigma_j\sigma_{ij}E_{\mathrm{PC},j}$. In analogy with the equation above, the nonlinear constitutive relation is given by[41]

$$\vec{J}^{(3)}_{-\omega}(\vec{r})=\int\int\int\vec{\vec{\Xi}}(\vec{r},\vec{r}',\vec{r}'',\vec{r}''') \vdots\vec{E}(\vec{r}''')\vec{E}(\vec{r}'')\vec{E}^*(\vec{r}')d^3r'''d^3r''d^3r', \tag{3}$$

where $\vec{\vec{\Xi}}(\vec{r},\vec{r}',\vec{r}'',\vec{r}''')=\vec{\vec{\Xi}}(\vec{r},\vec{r}',\vec{r}'',\vec{r}''';\omega)$ is the nonlocal single-electron conductivity tensor of the third order in the mixed space-frequency domain. The ith element of the third-order current density is obtained upon integration of $[\vec{\vec{\Xi}}\vdots\vec{E}\vec{E}\vec{E}^*]_i=\Sigma_{jkh}\Xi_{ijkh}E_hE_kE_j^*$ over the $\vec{r}'''$, $\vec{r}''$, and $\vec{r}'$ spaces. In Eq. (3), $\vec{E}(\vec{r})\equiv\vec{E}(\vec{r};\omega)$ denotes the local electric driving field.

The explicit expression for the linear nonlocal conductivity tensor $\overleftrightarrow{\sigma}(\vec{r},\vec{r}';\omega)$ is well known,[44] and may be calculated by various techniques. Starting for instance from the Liouville equation of motion for the density-matrix operator ρ, the linear current density is obtained from

$$\vec{J}^{(1)}_{-\omega}(\vec{r})=\mathrm{Tr}\{\rho^{(0)}\vec{J}^{(1)}_{-\omega}\}+\mathrm{Tr}\{\rho^{(1)}_{-\omega}\vec{J}^{(0)}\}, \tag{4}$$

where $\rho^{(0)}$ and $\rho^{(1)}_{-\omega}$ are the density-matrix operator in thermal equilibrium and its first-order perturbation at ω, respectively, and $\vec{J}^{(0)}$ and $\vec{J}^{(1)}_{-\omega}$ are the free part and the relevant vector-potential-dependent part (at ω) of the current-density operator. The quantity $\mathrm{Tr}\{\cdots\}$ in Eq. (4) denotes the trace of $\{\cdots\}$. From the expression found for the linear current density in this manner, the linear nonlocal conductivity tensor is readily extracted. The density-matrix operator approach is convenient also for a determination of the nonlinear part of the induced current density, thus obtaining

$$\vec{J}^{(3)}_{-\omega}(\vec{r})=\tfrac{1}{2}\mathrm{Tr}\{\rho^{(2)}_{-2\omega}\vec{J}^{(1)}_{\omega}\}+\mathrm{Tr}\{\rho^{(2)}_0\vec{J}^{(1)}_{-\omega}\}+\mathrm{Tr}\{\rho^{(3)}_{-\omega}\vec{J}^{(0)}\}, \tag{5}$$

in a notation where $\rho^{(2)}_0$ and $\rho^{(2)}_{-2\omega}$ denote the second-order dc and second-harmonic (2ω) parts of the density-matrix operator, respectively, and $\rho^{(3)}_{-\omega}$ is the third-order part at the fundamental frequency. From the explicit expression for $\vec{J}^{(3)}_{-\omega}(\vec{r})$ one can find the nonlinear conductivity response tensor. Details of the density-matrix calculation of $\vec{\vec{\Xi}}(\vec{r},\vec{r}',\vec{r}'',\vec{r}''';\omega)$ as well as the rather comprehensive formula for this quantity can be found in Ref. 41, where also a discussion of the microscopic physics behind this nonlinear response is given.

By inserting Eqs. (2) and (3) into Eq. (1), an integrodifferential equation is obtained for the phase conjugated field, in which the forced current density $\vec{J}^{(3)}_{-\omega}(\vec{r})$ can be considered as a prescribed quantity in the parametric approximation adopted in the following. Since only a small amount of the fundamental field, at least for single quantum-well systems studied here, is converted nonlinearly, the parametric approximation is justified.

B. Two-dimensional translational invariance

Considering a structure exhibiting two-dimensional translational invariance against displacements parallel to say the x-y plane, a bulklike material response is retained in two dimensions, and thus through conservation of pseudomomentum the concept of phase matching has to be fulfilled in the x-y plane.

In the above-mentioned system it is natural to express the various vector and tensor quantities in a mixed Fourier representation, where only the z coordinates are kept in real space. Each space coordinate $\vec{r}$ is then in the mixed Fourier representation transformed into a pair of $(z;\vec{q}_\parallel)$, where $\vec{q}_\parallel$ is the wave vector representation corresponding to the x-y representation in real space.

Performing a Fourier analysis in the x and y coordinates, the linear constitutive relation takes the form

$$\vec{J}^{(1)}_{-\omega}(z;\vec{q}_\parallel)=\int\overleftrightarrow{\sigma}(z,z';\vec{q}_\parallel)\cdot\vec{E}(z';\vec{q}_\parallel)dz'. \tag{6}$$

In the analysis of the nonlinear conductivity tensor in the mixed Fourier space described above, conservation of pseudomomentum (phase matching) in the direction parallel to the x-y plane appears directly from the general theory in the form

$$\vec{q}_\parallel'''+\vec{q}_\parallel''-\vec{q}_\parallel'-\vec{q}_\parallel=0. \tag{7}$$

This criterion implies that *if* we want the phase conjugated field to be counterpropagating to the probe field in the translationally invariant plane (as would be the natural choice when considering phase conjugation at all), then the two other (pump) fields *must* also be counterpropagating in this plane.

Thus limiting ourselves to the situation where the pump fields are counterpropagating, and assuming each of the interacting fields contains only one plane-wave component parallel to the x-y plane, the relevant nonlinear constitutive relation in the mixed Fourier representation takes the form

$$\vec{J}^{(3)}_{-\omega}(z;\vec{q}_\parallel)=\frac{1}{(2\pi)^4}\int\int\int \vec{\vec{\Xi}}(z,z',z'',z''';\vec{q}_\parallel,\vec{k}_\parallel) \vdots \vec{E}(z''';-\vec{k}_\parallel)\vec{E}(z'';\vec{k}_\parallel)\vec{E}^*(z';-\vec{q}_\parallel)dz'''dz''dz' + \text{i.t.}, \tag{8}$$

where $\vec{k}_\parallel$ is the parallel component of the wave vector associated with the pump fields, and $\vec{q}_\parallel$ is the parallel component of the wave vector associated with the probe and phase conjugated fields. The term ''i.t.'' denotes the so-called ''interchanged term,'' which is obtained from the first term by interchanging the two pump fields ($\vec{k}_\parallel$ replaced by $-\vec{k}_\parallel$). The reason that such a term has to be added arises from the fact that each of the electric fields basically consists of a sum of all three incoming fields, and that the phase conjugated term from the product of the three fields thus must include both permutations of the pump fields.

C. Phase conjugated field

After having sketched the calculation of the nonlinear DFWM response we turn our attention to the phase conjugated electric field. In the present case where the main parts of the interaction takes place in very small interaction volumes, we can expect that the generated phase conjugated field does not affect the dynamics of the pump and probe fields much, and thus take the parametric approximation.

Then from the linear constitutive relation and the wave equation we obtain the following integral equation for the phase conjugated field in the two-dimensional phase matching case[42]

$$\vec{E}_{\mathrm{PC}}(z;\vec{q}_\parallel,\omega)=\vec{E}^{\mathrm{B}}_{\mathrm{PC}}(z;\vec{q}_\parallel,\omega)-i\mu_0\omega\int\int \vec{\vec{G}}(z,z'';\vec{q}_\parallel,\omega) \cdot\vec{\vec{\sigma}}(z'',z';\vec{q}_\parallel,\omega)\cdot\vec{E}_{\mathrm{PC}}(z';\vec{q}_\parallel,\omega)dz''dz', \tag{9}$$

where $\vec{\vec{G}}(z,z'';\vec{q}_\parallel,\omega)$ is the so-called pseudovacuum propagator, and

$$\vec{E}^{\mathrm{B}}_{\mathrm{PC}}(z;\vec{q}_\parallel,\omega)=-i\mu_0\omega\int \vec{G}(z,z';\vec{q}_\parallel,\omega)\cdot\vec{J}^{(3)}_{-\omega}(z';\vec{q}_\parallel,\omega)dz' \tag{10}$$

is the nonlinear driving field [with $\vec{J}^{(3)}_{-\omega}(z';\vec{q}_\parallel,\omega)$ taken from Eq. (8)]. In the quantum-well case, the pseudovacuum propagator $\vec{\vec{G}}(z,z'';\vec{q}_\parallel,\omega)$ can be written as a sum of three terms

$$\vec{\vec{G}}(z,z';\vec{q}_\parallel,\omega)=\vec{\vec{D}}(z-z';\vec{q}_\parallel,\omega)+\vec{\vec{I}}(z+z';\vec{q}_\parallel,\omega)+\vec{\vec{g}}(z-z';\omega), \tag{11}$$

where the first two are named after the processes they describe. Thus the term $\vec{\vec{D}}(z-z';\vec{q}_\parallel,\omega)$ describes the direct propagation of the electromagnetic field from a source point at z' to the observation point at z. It is given by

$$\vec{\vec{D}}(z-z';\vec{q}_\parallel,\omega)=\frac{e^{iq_\perp|z-z'|}}{2iq_\perp}[\vec{e}_y\otimes\vec{e}_y+\Theta(z-z')\vec{e}_i\otimes\vec{e}_i+\Theta(z'-z)\vec{e}_r\otimes\vec{e}_r]. \tag{12}$$

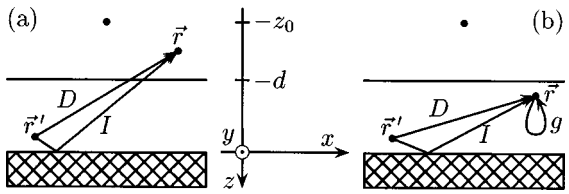

FIG. 1. The propagators appearing in the calculation of the phase conjugated field in the system we consider in this paper. The system consists of a three-layer thin-film structure, namely, vacuum, film (quantum well, extending from 0 to $-d$), and substrate (crosshatched). In the vacuum may be placed different kinds of sources, e.g., a quantum wire with its axis along the y direction (shown as a dot). In (a) the propagation of the electromagnetic field from a source point $\vec{r}'$ inside the quantum well to an observation point $\vec{r}$ outside the quantum well is shown, while in (b) the propagation of the electromagnetic field is illustrated in the case where both source and observation point are inside the quantum well. D is the propagation path described by the direct propagator, I is the propagation path described by the indirect propagator, and g denotes the self-field action propagator. In the center of the figure is shown the Cartesian coordinate system used in our calculations.

The indirect term, $\vec{\vec{I}}(z+z';\vec{q}_\parallel,\omega)$, describes the propagation from the source point of the part of the electromagnetic field that is going to the point of observation via the surface of the bulk medium. The expression for the indirect term reads

$$\vec{\vec{I}}(z+z';\vec{q}_\parallel,\omega)=\frac{e^{-iq_\perp(z+z')}}{2iq_\perp}[r^s\vec{e}_y\otimes\vec{e}_y+r^p\vec{e}_r\otimes\vec{e}_i]. \tag{13}$$

Finally, the self-field term characterizes the field generated at the observation point by the current density at the same point. The self-field part of the propagator is given by

$$\vec{\vec{g}}(z-z';\omega)=q^{-2}\delta(z-z')\vec{e}_z\otimes\vec{e}_z, \tag{14}$$

where $q=\omega/c_0$ is the vacuum wave number. In the above equations, $q_\perp=[q^2-q_\parallel^2]^{1/2}$, $\vec{e}_i=q^{-1}(q_\perp,0,-q_\parallel)$, and $\vec{e}_r=q^{-1}(-q_\perp,0,-q_\parallel)$, taking $\vec{q}_\parallel=q_\parallel\vec{e}_x$. The quantities r^s and r^p are the amplitude reflection coefficients of the vacuum/substrate interface in the absence of the quantum well. In general these are functions of $\vec{q}_\parallel$. The appropriate propagators for a single quantum-well system are shown in Fig. 1.

In a mesoscopic film the electric field generated via the direct and indirect processes at a given point is roughly speaking of the order $(\mu_0\omega/q_\perp)\int\vec{J}^{(3)}_{-\omega}dz'$, whereas the self-field has the magnitude $(\mu_0\omega/q^2)\vec{J}^{(3)}_{-\omega}$. Since $qd\ll 1$, where d is the thickness of the film, we judge the self-field term to dominate the phase conjugated field inside the quantum well, at least for single-level metallic quantum wells that have thicknesses on the atomic length scale. In the following we therefore use the so-called self-field approximation to calculate the phase conjugated field inside the quantum well. With the propagator $\vec{\vec{G}}(z,z';\vec{q}_\parallel,\omega)$ replaced by $\vec{\vec{g}}(z-z';\omega)$, the phase conjugated field fulfills the integral equation

$$\vec{E}_{\mathrm{PC}}(z;\vec{q}_{\parallel},\omega)=\vec{E}^{\mathrm{B}}_{\mathrm{PC}}(z;\vec{q}_{\parallel},\omega)+\frac{\vec{e}_z\otimes\vec{e}_z}{i\varepsilon_0\omega}\cdot\int\vec{\sigma}(z,z';\vec{q}_{\parallel},\omega)\cdot\vec{E}_{\mathrm{PC}}(z';\vec{q}_{\parallel},\omega)dz' \quad (15)$$

inside the well and the background field is now

$$\vec{E}^{\mathrm{B}}_{\mathrm{PC}}(z;\vec{q}_{\parallel},\omega)=\frac{\vec{e}_z\otimes\vec{e}_z}{i\varepsilon_0\omega}\cdot\vec{J}^{(3)}_{-\omega}(z;\vec{q}_{\parallel},\omega). \quad (16)$$

In the self-field approach the phase conjugated field has only a component perpendicular to the surface (the z component) inside the well and only the z component of the nonlinear current density $\vec{J}^{(3)}_{-\omega}$ drives the process.

Once the phase conjugated field inside the quantum well has been determined in a self-consistent manner from Eq. (15), it can be determined outside using Eq. (9). The self-field does not of course contribute to the exterior field, and no loop problem is involved. All that needs to be done is to integrate known quantities in the z direction over the well.

D. Nonlinear conductivity tensor

The nonlinear conductivity tensor appearing in Eq. (8) may in general be written as a sum of seven parts $(A-G)$ after the physical processes they describe. These have the tensor symmetries shown in Table I. In the present communication we use this conductivity tensor in the form it takes for media with two-dimensional translational invariance as it was developed by the present authors in a previous work,[41] but for quantum wells so thin that only a single bound level exists. The quantum well may be free standing, or it may be deposited on a substrate that can be described by a refractive index n relative to the vacuum on the other side of the film. The surface of the film is parallel to the x-y plane in a Cartesian coordinate system, and the interface between the film and the substrate is placed at $z=0$ as shown in Fig. 1. We further limit our study to the case where (i) all scattering takes place in the x-z plane, (ii) the interacting fields are linearly polarized in (p) or perpendicular to (s) the scattering plane, (iii) the pump fields in the phase conjugating system are counterpropagating monochromatic plane waves with a uniform amplitude along the z axis and propagating in a direction parallel to the x axis, and (iv) the field is calculated within the self-field approximation.

TABLE I. The tensor symmetries of the various parts $(A-G)$ of the DFWM conductivity. $\vec{J}_1-\vec{J}_4$ are four in general different vectors each obtained by a weighted superposition of single-particle transition current densities, and $\vec{e}_A=\vec{A}/A$.

DFWM Conductivity	Tensor symmetry
$\vec{\vec{\Xi}}^{A}(\vec{r},\vec{r}',\vec{r}'',\vec{r}''')$	$\vec{\vec{1}}\otimes\vec{\vec{1}}$
$\vec{\vec{\Xi}}^{B}(\vec{r},\vec{r}',\vec{r}'',\vec{r}''')$	$\vec{\vec{1}}\otimes\vec{J}_1\otimes\vec{J}_2$
$\vec{\vec{\Xi}}^{C}(\vec{r},\vec{r}',\vec{r}'',\vec{r}''')$	$\vec{e}_A\otimes\vec{\vec{1}}\otimes\vec{e}_A$
$\vec{\vec{\Xi}}^{D}(\vec{r},\vec{r}',\vec{r}'',\vec{r}''')$	$\vec{e}_A\otimes\vec{J}_1\otimes\vec{J}_2\otimes\vec{e}_A$
$\vec{\vec{\Xi}}^{E}(\vec{r},\vec{r}',\vec{r}'',\vec{r}''')$	$\vec{J}_1\otimes\vec{\vec{1}}\otimes\vec{J}_2$
$\vec{\vec{\Xi}}^{F}(\vec{r},\vec{r}',\vec{r}'',\vec{r}''')$	$\vec{J}_1\otimes\vec{J}_2\otimes\vec{\vec{1}}$
$\vec{\vec{\Xi}}^{G}(\vec{r},\vec{r}',\vec{r}'',\vec{r}''')$	$\vec{J}_1\otimes\vec{J}_2\otimes\vec{J}_3\otimes\vec{J}_4$

From (i) above we get a mirror plane at $y=0$, leaving only tensor elements of the conductivity tensors with an even number (0,2,4) of y's in the Cartesian index nonzero. Condition (iii) implies as a consequence of condition (ii) that no tensor elements of the nonlinear conductivity tensor with one or both of the last two Cartesian indices as x contributes to the phase conjugated response. Requirement (iv) above implies that the first Cartesian index of a tensor element should be z in order to contribute to the phase conjugated response. The choice of a single level quantum well in itself restricts the transition current density to contain x and y components only. Together with the fact that parts B and E give pure interband contributions, these choices leave two nonzero elements of the nonlinear conductivity tensor, namely,

$$\Xi^{C}_{zyyz}(z,z',z'',z''';q_{\parallel}-k_{\parallel})=\Xi^{C}_{zzzz}(z,z',z'',z''';q_{\parallel}-k_{\parallel})=\frac{e^4}{2^4\pi^2 i\hbar\omega^3 m_e^2}\,\mathcal{C}(q_{\parallel}-k_{\parallel})\,\delta(z'-z''')\,\delta(z-z'')\,|\psi(z')|^2|\psi(z)|^2, \quad (17)$$

$$\Xi^{D}_{zyyz}(z,z',z'',z''';q_{\parallel},k_{\parallel})=\frac{e^4}{2^6\pi^2 i\omega^3 m_e^3}\mathcal{D}(q_{\parallel},k_{\parallel})\,\delta(z-z''')\,|\psi(z'')|^2|\psi(z')|^2|\psi(z)|^2, \quad (18)$$

where

$$\mathcal{C}(q_{\parallel}-k_{\parallel})=2\int\frac{f(\vec{\kappa}_{\parallel}+[q_{\parallel}-k_{\parallel}]\vec{e}_x)-f(\vec{\kappa}_{\parallel})}{\hbar(q_{\parallel}-k_{\parallel})[2\kappa_x+q_{\parallel}-k_{\parallel}]/(2m_e)-i/\tau}d^2\kappa_{\parallel}, \quad (19)$$

$$\mathcal{D}(q_{\parallel},k_{\parallel})=2\int\frac{\kappa_y^2}{\hbar(q_{\parallel}+k_{\parallel})[2\kappa_x+q_{\parallel}+k_{\parallel}]/(2m_e)-i/\tau}\left(\frac{f(\vec{\kappa}_{\parallel})-f(\vec{\kappa}_{\parallel}+k_{\parallel}\vec{e}_x)}{\hbar k_{\parallel}[2\kappa_x+k_{\parallel}]/(2m_e)-i/\tau-\omega}+\frac{f(\vec{\kappa}_{\parallel}+[k_{\parallel}+q_{\parallel}]\vec{e}_x)-f(\vec{\kappa}_{\parallel}+k_{\parallel}\vec{e}_x)}{\hbar q_{\parallel}[2\kappa_x+q_{\parallel}+2k_{\parallel}]/(2m_e)-i/\tau+\omega}\right.$$
$$\left.+\frac{f(\vec{\kappa}_{\parallel})-f(\vec{\kappa}_{\parallel}+q_{\parallel}\vec{e}_x)}{\hbar q_{\parallel}[2\kappa_x+q_{\parallel}]/(2m_e)-i/\tau+\omega}+\frac{f(\vec{\kappa}_{\parallel}+[k_{\parallel}+q_{\parallel}]\vec{e}_x)-f(\vec{\kappa}_{\parallel}+q_{\parallel}\vec{e}_x)}{\hbar k_{\parallel}[2\kappa_x+k_{\parallel}+2q_{\parallel}]/(2m_e)-i/\tau-\omega}\right)d^2\kappa_{\parallel}. \quad (20)$$

The number 2 appearing in front of the integrals above represents the summation over the degenerate spin energies.

The free-particle character of the electron motion in the plane of the quantum well enables us to write the solutions to the light-unperturbed Schrödinger equation in the form $\Psi(\vec{r})=(2\pi)^{-1}\psi(z)\exp(i\vec{\kappa}_\parallel\cdot\vec{r})$, where $\vec{\kappa}_\parallel=(\kappa_x,\kappa_y,0)$ is the wave vector of the electron in consideration and $\psi(z)$, appearing in Eqs. (17) and (18), is the z-dependent part of the wave function, common to all electrons. The x-y-dependent parts of the wave functions, $(2\pi)^{-1}\exp(i\vec{\kappa}_\parallel\cdot\vec{r})$, are orthonormalized in the Dirac sense, i.e., $(2\pi)^{-2}\int\exp[i(\vec{\kappa}_\parallel-\vec{\kappa}'_\parallel)\cdot\vec{r}\,]d^2r=\delta(\vec{\kappa}_\parallel-\vec{\kappa}'_\parallel)$, and the z-dependent part fulfills the separate normalization condition $\int|\psi(z)|^2dz=1$. In Eqs. (19) and (20) the response of all electrons is taken into account by integrating over all possible $\vec{\kappa}_\parallel$ wave vectors. The eigenenergy $\mathcal{E}(\vec{\kappa}_\parallel)$ belonging to the state $\Psi(\vec{r}\,)$ is obtained by adding to the common bound-state energy ε, the kinetic energy in the parallel motion. Thus

$$\mathcal{E}(\vec{\kappa}_\parallel)=\varepsilon+\frac{\hbar^2}{2m_e}\kappa_\parallel^2. \tag{21}$$

The quantity $f(\vec{\kappa}_\parallel)=[1+\exp\{(\mathcal{E}(\vec{\kappa}_\parallel)-\mu)/(k_BT)\}]^{-1}$ denotes the Fermi-Dirac distribution function for this eigenstate, μ being the chemical potential of the electron system, k_B the Boltzmann constant, and T the absolute temperature.

E. Probe with single Fourier component

In the following we calculate the phase conjugated field generated by a probe field that consists of only one plane-wave component of wave vector $\vec{q}=(q_\parallel,0,q_\perp)$. A probe field of the form $\vec{E}(z;\vec{q}_\parallel)=\vec{E}e^{iq_\perp z}$ is hence inserted in Eq. (8).

Then, when using linearly polarized light, three different combinations of polarization gives a nonlinear current density, namely, (i) the one in which all participating fields are p polarized (ppp), and (ii) the two combinations where the pump fields are differently polarized and the probe field is s polarized (sps and pss). In all cases, the phase conjugated response is p polarized, and thus characterized in terms of the polarization states of the probe and phase conjugated fields, case (i) may be classified as a p to p transition, and cases (ii) as s to p transitions. A schematic illustration of these interaction configurations is shown in Fig. 2. Defining the z-independent quantity

$$\mathcal{J}^{(3)}_{-\omega,z}(\vec{q}_\parallel)\equiv\frac{J^{(3)}_{-\omega,z}(z;\vec{q}_\parallel)}{|\psi(z)|^2}, \tag{22}$$

the above conditions yields for the p to p transition

$$\mathcal{J}^{(3)}_{-\omega,z}(\vec{q}_\parallel)=\frac{e^4}{2^8\pi^6i\hbar\omega^3m_e^2}[\mathcal{C}(q_\parallel-k_\parallel)+\mathcal{C}(q_\parallel+k_\parallel)]\times E_z^{(1)}E_z^{(2)}E_z^*\int|\psi(z')|^2e^{-iq_\perp^{*}z'}dz' \tag{23}$$

and for the s to p transitions

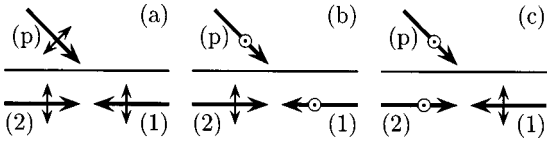

FIG. 2. Schematic illustration showing three of the possible field polarization combinations that may give rise to a phase conjugated response in a single level quantum well, viz. (a) the purely p-polarized configuration, and (b)–(c) the mixed polarization configurations where the pump fields are differently polarized while the probe is s polarized. The two mixed polarization states are closely related, since replacing $\vec{q}_\parallel$ with $-\vec{q}_\parallel$ in one of them yields the other. In both the (a) and (b)–(c) cases, the phase conjugated response is p polarized. The schemes are shown in the Cartesian coordinate system given in Fig. 1, such that the small arrows in the plane represent p-polarized states and the circles represent s-polarized states. The large arrows show the direction of (one Fourier component of) the wave vectors of the pump fields (1 and 2) and the probe field (p).

$$\mathcal{J}^{(3)}_{-\omega,z}(\vec{q}_\parallel)=\frac{e^4}{2^8\pi^6i\hbar\omega^3m_e^2}\left[\mathcal{C}(q_\parallel+k_\parallel)+\frac{\hbar}{4m_e}\mathcal{D}(\vec{q}_\parallel,-\vec{k}_\parallel)\right]\times E_y^{(1)}E_z^{(2)}E_y^*\int|\psi(z')|^2e^{-iq_\perp^{*}z'}dz', \tag{24}$$

$$\mathcal{J}^{(3)}_{-\omega,z}(\vec{q}_\parallel)=\frac{e^4}{2^8\pi^6i\hbar\omega^3m_e^2}\left[\mathcal{C}(q_\parallel-k_\parallel)+\frac{\hbar}{4m_e}\mathcal{D}(q_\parallel,k_\parallel)\right]\times E_z^{(1)}E_y^{(2)}E_y^*\int|\psi(z')|^2e^{-iq_\perp^{*}z'}dz'. \tag{25}$$

In the above three equations, the superscript (1) refers to the pump field propagating along the x axis in the positive direction ($\vec{k}_\parallel=k_\parallel\vec{e}_x$), and the superscript (2) refers to the other pump field. The s to p transitions are symmetric in the sense that if the probe wave vector $\vec{q}_\parallel$ is replaced by $-\vec{q}_\parallel$ in Eq. (24), then the result of Eq. (25) is obtained, and vice versa. The p to p transition is symmetric to itself in this sense.

For a single-level quantum well, the zz component of the linear conductivity tensor is given by[44]

$$\sigma_{zz}(z,z';\vec{q}_\parallel)=\frac{ie^2\mathcal{N}}{m_e(\omega+i/\tau)}|\psi(z)|^2\delta(z-z'), \tag{26}$$

where

$$\mathcal{N}=\frac{2}{(2\pi)^2}\int f(\vec{\kappa}_\parallel)d^2\kappa_\parallel. \tag{27}$$

In order to take into account the coupling to the surroundings we have introduced a phenomenological relaxation time τ in the diamagnetic expression for σ_{zz} [Eq. (26)].[44] A factor of 2 in this equation again stems from the spin summation, and the quantity $\mathcal{N}|\psi(z)|^2$ is the conduction electron density. The phase conjugated field inside the quantum well has a z component, $E_{PC,z}(z;\vec{q}_\parallel)$, only, and by combining Eqs. (15), (16), and (26) it appears that this is given by

$$E_{\mathrm{PC},z}(z;\vec{q}_\parallel)=\frac{im_e(\omega+i/\tau)}{e^2\mathcal{N}|\psi(z)|^2-\epsilon_0 m_e\omega(\omega+i/\tau)}J^{(3)}_{-\omega,z}(z;\vec{q}_\parallel). \tag{28}$$

Using now Eq. (9), the z components of the phase conjugated field outside the quantum well can be calculated, and the result is

$$E_{\mathrm{PC},z}(z;\vec{q}_\parallel)=\mathcal{J}^{(3)}_{-\omega,z}(\vec{q}_\parallel)e^{-iq_\perp z}\frac{q_\parallel^2 m_e(\omega+i/\tau)}{2q_\perp}\times\int\frac{(e^{iq_\perp z'}+r^p e^{-iq_\perp z'})|\psi(z')|^2}{e^2\mathcal{N}|\psi(z')|^2-\epsilon_0 m_e\omega(\omega+i/\tau)}dz', \tag{29}$$

where the relevant expression for $\mathcal{J}^{(3)}_{-\omega,z}(\vec{q}_\parallel)$ is taken from Eq. (23), (24), or (25). Given the z component of the phase conjugated field, the x component may be found from

$$E_{\mathrm{PC},x}(z;\vec{q}_\parallel)=\frac{q_\perp}{q_\parallel}E_{\mathrm{PC},z}(z;\vec{q}_\parallel), \tag{30}$$

which follows from the expression for the electromagnetic propagator, or equivalently from the demand that the phase conjugated field must be transverse in vacuum.

The integral in Eq. (29) is different from zero only in the region of the quantum well [from approximately $z'=-d$ to approximately $z'=0$ in the chosen coordinate system, the exact domain depending on the extent of the electronic wave function $\psi(z')$]. Since the width ($\sim d$) of a single-level metallic quantum well is in the Ångström range, and $q_\perp$ is typically in the micrometer range for optical signals such that $q_\perp d\ll 1$, it is a good approximation to put $\exp(\pm iq_\perp z')=1$ in Eq. (29). For electromagnetic frequencies so high that $q_\perp\sim d^{-1}$, the present theory would in any case be too simple to rely on [the Bloch function character of the wave functions along the surface and excitation to the continuum (photoemission, etc.) should be incorporated at least]. With the above-mentioned approximation, Eq. (29) is reduced to

$$E_{\mathrm{PC},z}(z;\vec{q}_\parallel)=\mathcal{J}^{(3)}_{-\omega,z}(\vec{q}_\parallel)e^{-iq_\perp z}\frac{(1+r^p)q_\parallel^2}{2\epsilon_0\omega q_\perp}\times\int\frac{|\psi(z')|^2}{\gamma|\psi(z')|^2-1}dz', \tag{31}$$

where $\gamma=e^2\mathcal{N}/[\epsilon_0 m_e\omega(\omega+i/\tau)]$. Using the approximation $\exp(iq_\perp z')=1$ and the normalization condition on $\psi(z')$, Eqs. (23)–(25) are reduced to

$$\mathcal{J}^{(3)}_{-\omega,z}(\vec{q}_\parallel)=\frac{e^4}{2^8\pi^6 i\hbar\omega^3 m_e^2}[\mathcal{C}(q_\parallel-k_\parallel)+\mathcal{C}(q_\parallel+k_\parallel)]\times E_z^{(1)}E_z^{(2)}E_z^*, \tag{32}$$

$$\mathcal{J}^{(3)}_{-\omega,z}(\vec{q}_\parallel)=\frac{e^4}{2^8\pi^6 i\hbar\omega^3 m_e^2}\left[\mathcal{C}(q_\parallel+k_\parallel)+\frac{\hbar}{4m_e}\mathcal{D}(\vec{q}_\parallel,-\vec{k}_\parallel)\right]\times E_y^{(1)}E_z^{(2)}E_y^*, \tag{33}$$

and

$$\mathcal{J}^{(3)}_{-\omega,z}(\vec{q}_\parallel)=\frac{e^4}{2^8\pi^6 i\hbar\omega^3 m_e^2}\left[\mathcal{C}(q_\parallel-k_\parallel)+\frac{\hbar}{4m_e}\mathcal{D}(q_\parallel,k_\parallel)\right]\times E_z^{(1)}E_y^{(2)}E_y^*, \tag{34}$$

respectively.

Thus the phase conjugated field from a single-level quantum well is described in the mixed Fourier space by Eq. (31) with insertion of Eq. (32), (33), or (34), the expressions for $\mathcal{C}$ [Eq. (19)] and $\mathcal{D}$ [Eq. (20)] carrying the information on the two-dimensional electron dynamics.

So far, the description of the phase conjugated response has been independent of the actual wave functions in the active medium, and thus independent of the form of the quantum-well potential. In order to prepare our theory for a numerical study we now introduce a model potential in our quantum-well system, namely, the infinite barrier potential.

F. Infinite barrier model

To achieve a qualitative impression of the phase conjugation from a single-level metallic quantum well it is sufficient to carry out numerical calculations on the basis of the simple IB model. In this model the one-dimensional potential $V(z)$ is taken to be zero in the interval $-d\leqslant z\leqslant 0$ (inside the quantum well) and infinite elsewhere. The stationary-state wave function now is given by $\psi(z)=\sqrt{2/d}\sin(\pi z/d)$ inside the well and $\psi(z)=0$ outside, and the associated energy is $\varepsilon=(\pi\hbar)^2/(2m_e d^2)$. In the IB model the number of bound states is of course infinite, and to use this model in the context of a single-level calculation, one must be sure that only one of the bound states (the ground state) has an energy below the Fermi energy, and that the optical frequency is so low that interlevel excitations are negligible.

For a metallic quantum well one may even at room temperature approximate the Fermi-Dirac distribution function appearing in the expressions for $\mathcal{C}$, $\mathcal{D}$, and $\mathcal{N}$ in Eqs. (19), (20), and (27) by its value at zero temperature, i.e.,

$$\lim_{T\to 0}f(\vec{\kappa}_\parallel)=\Theta\left\{\mathcal{E}_F-\frac{\hbar^2}{2m_e}\left[\left(\frac{\pi}{d}\right)^2+\kappa_\parallel^2\right]\right\}, \tag{35}$$

where Θ is the Heaviside step function and $\mathcal{E}_F$ is the Fermi energy of the system. In the low-temperature limit it is possible to find analytical solutions to the integrals over $\vec{\kappa}_\parallel$ appearing in Eqs. (19) and (20). This is adequately achieved by performing a coordinate transformation into cylindrical coordinates, since each Heaviside step function gives nonzero values in the κ_x-κ_y space only inside a circle with radius, say, α. The explicit calculations are tedious but trivial to carry out, and since the final expressions for $\mathcal{C}$ and $\mathcal{D}$ are rather long we do not present them here. For the interested reader some steps in the calculations are reproduced in the Appendix.

The Fermi energy is calculated from the global charge neutrality condition,[42] which for a single-level quantum well takes the form

$$\mathcal{N}=ZN_+d, \tag{36}$$

where N_+ is the number of positive ions per unit volume and Z is the valence of these ions. Since $\mathcal{N}=m_e(\mathcal{E}_F-\varepsilon)/(\pi\hbar^2)$, cf. the calculation in the Appendix, one gets

$$\mathcal{E}_F=\frac{\pi\hbar^2}{m_e}\left[ZN_+d+\frac{\pi}{2d^2}\right]. \tag{37}$$

In order that just the ground state (energy ε) has an energy less than the Fermi energy, the film thickness must be less than a certain maximum value $d_{\max}$. When the thickness of the well becomes so large that the Fermi energy equals the energy $\varepsilon_2=(2\pi\hbar)^2/(2m_ed^2)$ of the first excited state a second bound state of energy less than $\mathcal{E}_F$ will appear. From the condition $\mathcal{E}_F(d_{\max})=\varepsilon_2(d_{\max})$, $d_{\max}$ can be calculated, and one gets by means of Eq. (37)

$$d_{\max}=\sqrt[3]{3\pi/(2ZN_+)}, \tag{38}$$

i.e., a result that depends on the number of conduction electrons in the film. The minimum thickness is in the IB model zero, but in reality the smallest thickness is a single monolayer.

Inserting the IB model into the integral over the source region appearing in Eq. (31) we get

$$\int \frac{|\psi(z')|^2}{\gamma|\psi(z')|^2-1}dz'=\int_{-d}^{0}\frac{2\sin^2\left(\frac{\pi z'}{d}\right)}{2\gamma\sin^2\left(\frac{\pi z'}{d}\right)-d}dz', \tag{39}$$

which by substitution of $\theta=\pi z'/d$, addition and subtraction of d in the nominator of the integral, and use of $2\gamma\sin^2\theta-d=2\gamma[\sqrt{1-d/(2\gamma)}-\cos\theta][\sqrt{1-d/(2\gamma)}+\cos\theta]$ gives

$$\frac{d}{\pi\gamma}\left[\pi-\frac{d}{4\gamma}\frac{1}{\sqrt{1-d/(2\gamma)}}\int_0^{2\pi}\frac{d\theta}{\sqrt{1-d/(2\gamma)}+\cos\theta}\right]=\frac{d}{\gamma}\left[1-\frac{1}{\sqrt{2\gamma/d-1}}\right]\approx\frac{d}{\gamma}. \tag{40}$$

The solution to the integral in Eq. (40) is obtained by use of Eq. (A13), and since $2|\gamma|/d\gg1$ the last approximation follows [for metals, $|\gamma|$ lies typically between 1 and 100 in the optical region (e.g., for copper $|\gamma|\approx85$ in the present study) and d is in the Ångström range]. Using this result and the expression for the Fermi energy given in Eq. (37), we obtain by insertion into Eq. (31) the result

$$E_{\mathrm{PC},z}(z;\vec{q}_\parallel)=\frac{q_\parallel^2m_e(\omega+i/\tau)(1+r^p)}{2q_\perp e^2ZN_+}\mathcal{J}^{(3)}_{-\omega,z}(\vec{q}_\parallel)e^{-iq_\perp z}. \tag{41}$$

By insertion of the relevant expressions for $\mathcal{J}^{(3)}_{-\omega,z}(\vec{q}_\parallel)$ we finally obtain the following results for the z component of the phase conjugated field outside the quantum well:

$$E_{\mathrm{PC},z}(z;\vec{q}_\parallel)=\frac{e^2(\omega+i/\tau)(1+r^p)}{2^9\pi^6\hbar\omega^3ZN_+m_e}\frac{q_\parallel^2}{iq_\perp}[\mathcal{C}(q_\parallel-k_\parallel)+\mathcal{C}(q_\parallel+k_\parallel)]E_z^{(1)}E_z^{(2)}E_z^*e^{-iq_\perp z}, \tag{42}$$

for the purely p-polarized configuration, and

$$E_{\mathrm{PC},z}(z;\vec{q}_\parallel)=\frac{e^2(\omega+i/\tau)(1+r^p)}{2^9\pi^6\hbar\omega^3ZN_+m_e}\frac{q_\parallel^2}{iq_\perp}\left[\mathcal{C}(q_\parallel+k_\parallel)+\frac{\hbar}{4m_e}\mathcal{D}(q_\parallel,-k_\parallel)\right]E_y^{(1)}E_z^{(2)}E_y^*e^{-iq_\perp z}, \tag{43}$$

$$E_{\mathrm{PC},z}(z;\vec{q}_\parallel)=\frac{e^2(\omega+i/\tau)(1+r^p)}{2^9\pi^6\hbar\omega^3ZN_+m_e}\frac{q_\parallel^2}{iq_\perp}\left[\mathcal{C}(q_\parallel-k_\parallel)+\frac{\hbar}{4m_e}\mathcal{D}(q_\parallel,k_\parallel)\right]E_z^{(1)}E_y^{(2)}E_y^*e^{-iq_\perp z} \tag{44}$$

for the configurations with mixed polarization of the pump fields. The x component of the phase conjugated field is obtained using Eq. (30).

III. NUMERICAL RESULTS

The theoretical description presented in the previous section resulted in expressions for the phase conjugated field from a single-level quantum well. Thus for the numerical work, the phase conjugated field is given completely by Eqs. (42)–(44) and (30) with the insertion of the expressions for the electron dynamics parallel to the surface plane, given by Eqs. (A17)–(A18) in the Appendix. In the following we will present the phase conjugation reflection coefficient, succeeded by a discussion of a possible excitation scheme that might be adequate for studies of phase conjugation of optical near fields.[45]

A. Phase conjugation reflection coefficient

To estimate the amount of light we get back through the phase conjugated channel, we define the phase conjugation (energy) reflection coefficient as

$$R_{\mathrm{PC}}(z;\vec{q}_\parallel)=\frac{I_{\mathrm{PC}}(z;\vec{q}_\parallel)}{I^{(1)}I^{(2)}I_{\mathrm{probe}}(-d;\vec{q}_\parallel)}, \tag{45}$$

in which $I^{(1)}$, $I^{(2)}$, I_{probe}, and I_{PC} are the intensities of the two pump beams, the probe, and the phase conjugated field, respectively. Each of the intensities are given by

$$I=\frac{\epsilon_0c_0}{2}\frac{\vec{E}\cdot\vec{E}^*}{(2\pi)^4}, \tag{46}$$

where the factor of $(2\pi)^{-4}$ originates from the manner in which we have introduced the Fourier amplitudes of the

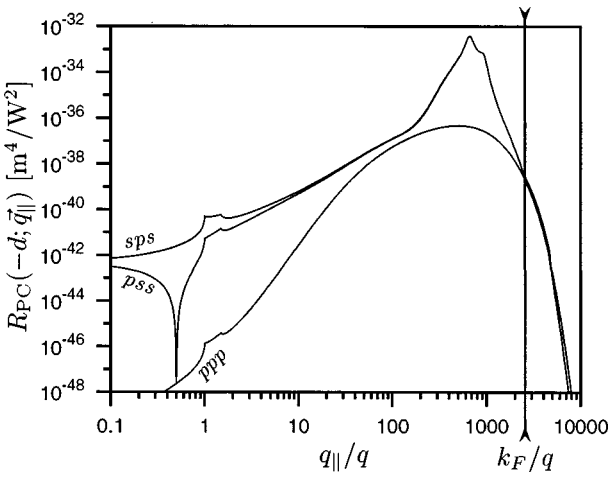

FIG. 3. The phase conjugation reflection coefficient at the vacuum/film interface, $R_{\mathrm{PC}}(-d;\vec{q}_\parallel)$, is plotted for (ppp) the p to p transition [corresponding to Fig. 2(a)], (sps) one of the s to p transitions [corresponding to Fig. 2(b)], and (pss) the other s to p transition [corresponding to Fig. 2(c)], as a function of the normalized component of the probe wave vector along the interface, $q_\parallel/q$. The normalized Fermi wave number is indicated by the vertical line.

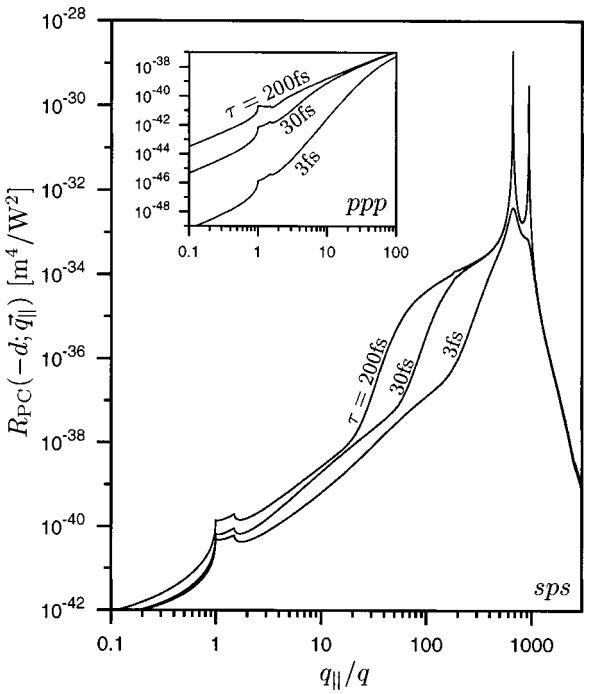

FIG. 4. The phase conjugation reflection coefficient at the surface of the phase conjugator is plotted for different values ($\tau \in \{200,30,3\}$ femtoseconds) of the relaxation time. The main figure shows the result for the sps configuration, while the inset shows the ppp result.

fields. If the probe field is evanescent the intensity of the phase conjugated field, $I_{\mathrm{PC}}(z;\vec{q}_\parallel)$, will depend on the distance from the surface, and consequently the reflection coefficient is z dependent in such a case.

For the remaining part of this work we choose a copper quantum well with $N_+ = 8.47\times10^{28}$ m^{-3} and $Z=1$ (data taken from Ref. 46). Then from Eq. (38), the maximal thickness becomes $d_{\max}=3.82$ Å, which is more than two monolayers and less than three. Thus we have two obvious choices for the thickness of the quantum well, namely, a single monolayer or two monolayers. We choose two monolayers, corresponding to a thickness of $d=3.6$ Å. The Cu quantum well can adequately be deposited on a glass substrate for which we use a refractive index n of 1.51. With this substrate, a reasonable description of the linear vaccum/substrate amplitude reflection coefficient r^p is obtained by use of the classical Fresnel formula

$$r^p=\frac{n^2q_\perp-(n^2q^2-q_\parallel^2)^{1/2}}{n^2q_\perp+(n^2q^2-q_\parallel^2)^{1/2}}, \tag{47}$$

$q=\omega/c_0$ being the vacuum wave number, as before. Then, having the pump fields parallel to the x axis gives a pump wave number $k_\parallel=1.51q$. The wavelength λ of the light is chosen to be $\lambda=1061$ nm.

The phase conjugation reflection coefficient at the vacuum/film interface, $R_{\mathrm{PC}}(-d;\vec{q}_\parallel)$ is plotted in Fig. 3 as a function of the parallel component $(q_\parallel)$ of the wave vector for both the p to p transition and the two s to p transitions. The reason that the two curves for the s to p transitions appear the same in the high end of the $q_\parallel/q$ spectrum is that for $k_\parallel \ll q_\parallel$ we have $\mathcal{C}(q_\parallel-k_\parallel)\simeq\mathcal{C}(q_\parallel+k_\parallel)$ and $\mathcal{D}(q_\parallel,k_\parallel)\simeq\mathcal{D}(q_\parallel,-k_\parallel)$. The ''bubble'' appearing on the sps and pss curves from around $q_\parallel/q\sim100$ to $q_\parallel/q\sim k_F/q$ is due to the two-dimensional electron dynamics hidden in $\mathcal{D}(q_\parallel,k_\parallel)$. To be a little more specific, the left of the two peaks stems from the second term, while the peak to the right in the bubble stems from the third term.

To illustrate the similarity between the two possible s to p transitions, we can take Eq. (43) to describe the phase conjugated field, which for positive values of $q_\parallel/q$ gives the result in Fig. 3 (sps). Using the other s to p transition, given by Eq. (44), we get instead the result in Fig. 3 (pss) for positive values of $q_\parallel/q$. The symmetry between the two configurations is obtained by looking at the negative values of $q_\parallel/q$, since Eq. (43) plotted for negative values of $q_\parallel/q$ gives the (pss) curve in Fig. 3. Similarly, by starting with Eq. (44), the resulting curve for negative values of $q_\parallel/q$ gives the (sps) result in Fig. 3.

The choice of an adequate relaxation time τ is a difficult problem and it appears from Fig. 4 that the value of the relaxation time has a great impact on the phase conjugation reflection coefficient. We have plotted the reflection coefficent for three values of the relaxation time, namely, (i) 30 fs and (ii) 200 fs, which are typical values one would find for bulk copper[46] at (i) room temperature and (ii) at 77 K, and (iii) 3 fs. The value in case (iii) is obtained by a conjecture based on the difference between measured data for a lead quantum well[47] and the bulk value for lead at room temperature. The difference between the relaxation time measured by Jalochowski, Stróżak, and Zdyb[47] is for two monolayers approximately one order of magnitude. Based on the results of Jalochowski, Strozak, and Zdyb[47] we have for the data presented in this work chosen the value of the relaxation time to be 3 fs. As it can be seen from Fig. 4, the bubble in the curve corresponding to the sps configuration appears earlier in the

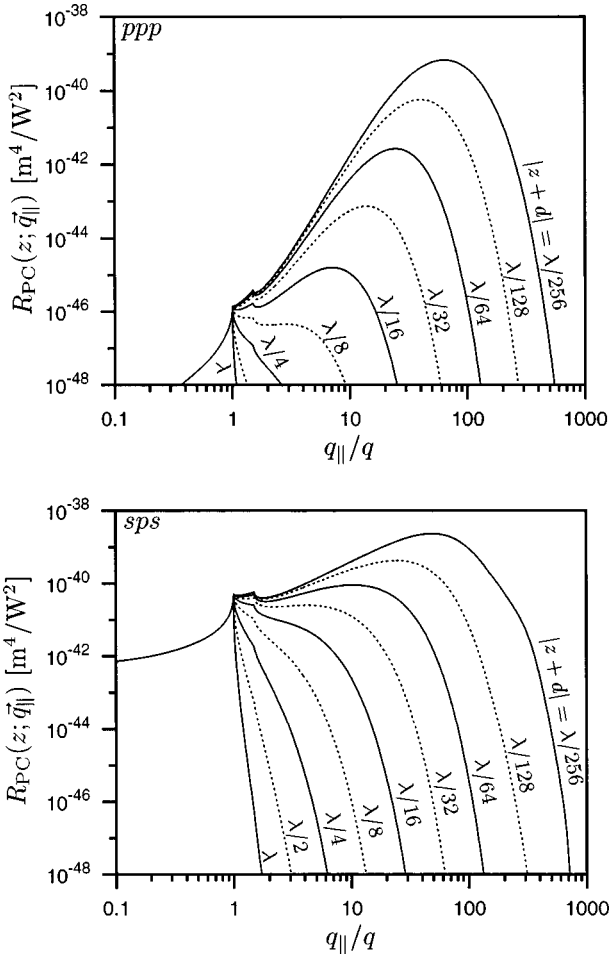

FIG. 5. The $q_\parallel/q$ dependence of the phase conjugation reflection coefficient, $R_{PC}(z;\vec{q}_\parallel)$, is plotted at different distances $|z+d| \in \{\lambda, \lambda/2, \lambda/4, \lambda/8, \lambda/16, \lambda/32, \lambda/64, \lambda/128, \lambda/256\}$ from the vacuum/film interface. The upper figure shows the results for the p to p transition. The lower figure shows the results for the s to p transition that corresponds to Fig. 2(b).

$q_\parallel/q$ spectrum for higher values of τ. For the ppp configuration the lower end of the spectrum is damped when τ becomes smaller.

We have in Fig. 5 plotted the phase conjugation reflection coefficient for the p to p transition and one of the s to p transitions, respectively, for different distances from the surface of the phase conjugator. Due to our particular interest in the phase conjugation of the evanescent modes in the Fourier spectrum the chosen distances are fractions of the vacuum wavelength. In Fig. 6 we have plotted the part of the Fourier spectrum for all three configurations that is judged to be the most easily accessible to single-mode excitation in experimental investigations.

It appears from Fig. 5 (ppp) that the phase conjugation reflection coefficient is independent of the distance from the metal film in the region where $q_\parallel/q \leqslant 1$. This is so because the probe field, and hence also the phase conjugated field, are of propagating character ($q_\perp = [q^2 - q_\parallel^2]^{1/2}$ is real). In the region where $q_\parallel/q > 1$, both the probe field and the phase conjugated field are evanescent ($q_\perp = i[q_\parallel^2 - q^2]^{1/2}$ is a purely imaginary quantity), and in consequence the reflection coefficient decreases rapidly with the distance from the phase

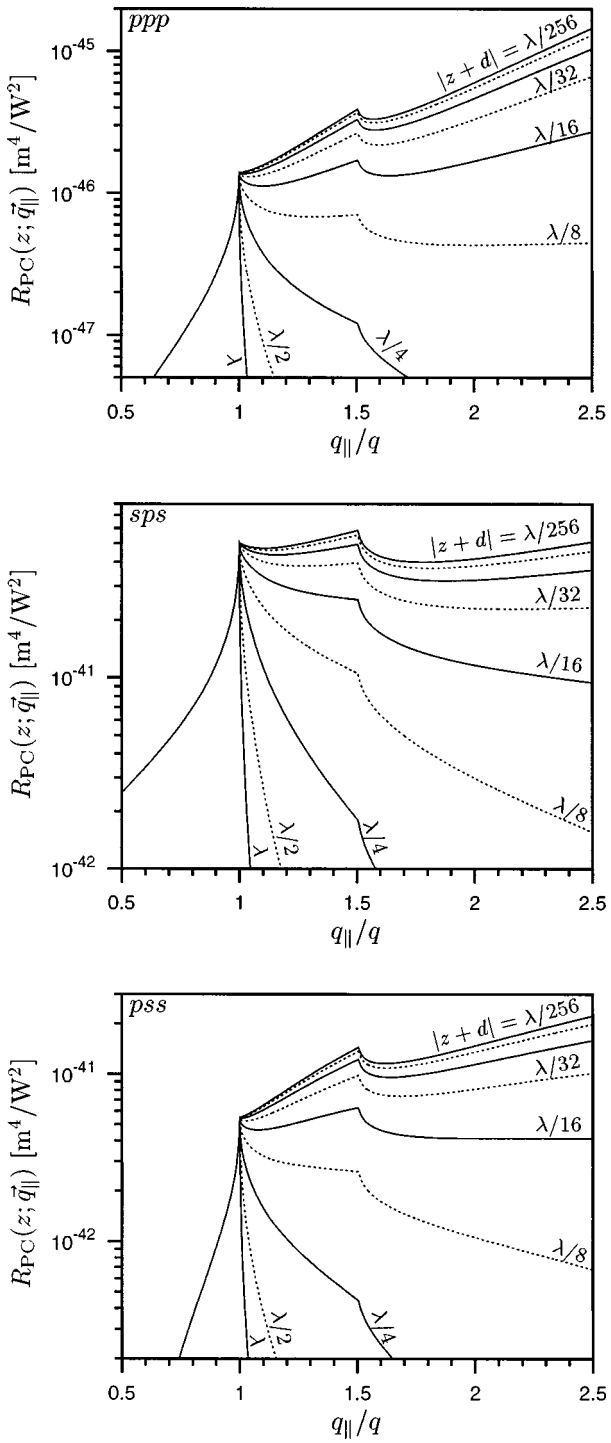

FIG. 6. The phase conjugation reflection coefficient, $R_{PC}(z;\vec{q}_\parallel)$, is plotted at different distances $|z+d| \in \{\lambda, \lambda/2, \lambda/4, \lambda/8, \lambda/16, \lambda/32, \lambda/64, \lambda/128, \lambda/256\}$ from the vacuum/film interface as a function of the normalized probe wave number $q_\parallel/q$. Results are shown for the three polarization combinations ppp, sps, and pss in the range where we expect single mode excitation to be experimentally feasible.

conjugator. Already a single wavelength away from the surface of the phase conjugator the evanescent modes of the phase conjugated field have essentially vanished and only propagating modes are detectable. Although the evanescent Fourier components of the phase conjugated field are present only less than an optical wavelength from the surface, this

does not imply that the nonlinear mixing of the electromagnetic waves is less effective in the regime of the evanescent modes. It is in fact the opposite, as may be seen, for instance, from Fig. 3. The maximum coupling for the p to p transition is obtained for $q_\parallel/q \simeq 500$, and in comparison with R_{PC} at $q_\parallel/q \simeq 1$, the maximum in R_{PC} is nine orders of magnitude larger, and, respectively, seven and eight orders of magnitude larger for the two s to p transitions, which have their maxima at around $q_\parallel/q \simeq 700$. As we observe from Fig. 5, as the distance from the film increases the maximum value decreases and is shifted downwards in the $q_\parallel/q$ spectrum. But only when the distance from the phase conjugator becomes larger than $\sim\lambda/10$ (ppp) respectively $\sim\lambda/60$ (sps), the phase conjugated signal is largest at $q_\parallel/q \approx 1$.

The absolute value of the reflection coefficients may seem very small, but utilizing a high-power Nd:YAG laser with, say an energy of 100 mJ per pulse available for each of the three incoming fields, a pulse (assumed square for simplicity) duration of 4 ns, and an interaction area of 25 mm^2, the intensity of each of these fields will be of the order of $1\,\mathrm{TW/m}^2$, and the phase conjugated intensity lies between 100 $\mathrm{pW/m}^2$ and 1 $\mathrm{W/m}^2$ in the full range of $q_\parallel/q$ for which the reflection coefficient has been plotted in Fig. 5 (ppp), and between 1 $\mu\mathrm{W/m}^2$ and 1 $\mathrm{kW/m}^2$ in relation to the data in Fig. 5 (sps).

In many theoretical studies of the properties of phase conjugated fields it is assumed that the phase conjugator is ideal.[37–39] By this is meant that the phase conjugation reflection coefficient is independent of the angle of incidense of the (propagating) probe field (and maybe also of the state of polarization). In the present case, the ideal phase conjugator assumption is certainly not good. Prior to the observation that evanescent fields could be phase conjugated[45] it was often assumed in theory[48] that $R_{\mathrm{PC}}=0$ in the region $q_\parallel/q>1$, and in later studies[38,39] it has been assumed that also the phase conjugation of evanescent waves is ideal, i.e., independent of $q_\parallel/q(\gtrsim 1)$. When it comes to the phase conjugation from quantum-well systems our analysis indicates that use of an energy reflection coefficient independent of $q_\parallel/q$ in general is bad. Only at specific distances the ideal phase conjugator assumption might be justified, see e.g., the results representing R_{PC} at $|z+d|=\lambda/8$ in Fig. 6 (ppp). The kink in the reflection coefficient (which is most pronounced close to the metal/vacuum interface) found at $q_\parallel/q=n(=1.51)$ appears when the probe field changes from being propagating to being evanescent inside the substrate.

Above we have discussed the nonlinear reflection coefficient for the p to p configuration. It appears from Figs. 5 and 6 that the quantitative picture is the same for the s to p cases, though the reflection coefficient for the s to p transitions roughly speaking are five orders of magnitude larger in the experimentally most adequate evanescent region of the Fourier spectrum $(1\lesssim q_\parallel/q\lesssim 2.5)$ for single mode excitation.

The IB model only offers a crude description of the electronic properties of a quantum well. Among other things, the electron density profile at the ion/vacuum edge is poorly accounted for in this model, which gives too sharp a profile and underestimates the spill-out of the wave function. Altogether one should be careful to put too much reality into the IB model when treating local-field variations (related to, say, $q_\parallel$ or $q_\perp$) on the atomic length scale. Also the neclect of the Bloch character of the wave functions accounting for the dynamics in the plane of the well is doubtful in investigations of the local field among the atoms of the quantum well. The crucial quantity in the above-mentioned context is the Fermi wave number $k_F=(2m_e\mathcal{E}_F)^{1/2}/\hbar$, and in relation to Fig. 5, only results for $q_\parallel/q$ ratios less than approximately

$$\frac{k_F}{q}=\lambda\sqrt{\frac{ZN_+d}{2\pi}+\frac{1}{4d^2}}, \tag{48}$$

appears reliable. Insertion of the appropriate values for two monolayers of copper: $ZN_+=8.47\times10^{28}$ m^{-3}, $d=3.6$ Å, and the wavelength $\lambda=1061$ nm gives $k_F=2.76\times10^3 q$. The data presented in Fig. 5 should therefore be well within this limit of our model.

Returning to the curve in Fig. 5 (ppp), which represents the reflection coefficient closest to the surface of the phase conjugator $(|z+d|=\lambda/256)$ one finds approximately a relation of the form $R_{\mathrm{PC}}=b(q_\parallel/q)^a$ with $a\simeq 5$ in the lower wave-number end of the evanescent region. The falloff of R_{PC} with $q_\parallel/q$ after the maximum (located at $q_\parallel/q\sim 50$) is much stronger than the increase towards the maximum. As the distance from the phase conjugator is increased the value of a gradually decreases. In Fig. 5(b) we observe a similar behavior, but this time the value of a in the approximate relation in the low end of the evanescent part of the Fourier spectrum is smaller, namely, $a\simeq 1.5$.

The energy reflection coefficient calculated at the vacuum/quantum-well interface, $R_{\mathrm{PC}}(-d;\vec{q}_\parallel)$, characterizes the effectiveness with which a given $(q_\parallel)$ plane-wave probe field (propagating or evanescent) may be phase conjugated, and the results presented in Fig. 3 indicate that this effectiveness (nonlinear coupling) is particularly large for (part of the) evanescent modes. The maximum in the effectivity is reached for a value of $q_\parallel/q$ as large as ~ 500–700. The strong coupling in part of the evanescent region does not necessarily reflect itself in any easy manner experimentally. First of all, one must realize that the strong-coupling effect may only be observed close to the quantum well, i.e., at distances $z\lesssim\lambda$. Secondly, one must be able to produce evanescent probe fields with relatively large values of $q_\parallel/q$. This is in and of itself by no means simple outside the range where the standard Otto[49,50] (or possibly Kretschmann)[51,52] techniques can be adopted. Roughly speaking, this range coincides with the ones shown in Fig. 6. To create probe fields with larger $q_\parallel/q$ values other kinds of experimental techniques must be used, and in the following we shall consider a particular example and in a qualitative manner discuss the resulting Fourier spectrum of the phase conjugated field.

B. Phase conjugated response using a wire source

In near-field optics evanescent fields with relatively large values of $q_\parallel/q$ are produced by various methods, all aiming at compressing the source field to subwavelength spatial extension (see, e.g., Refs. 53 and 54). From a theoretical point of view the radiation from a subwavelength source may in some cases be modeled by the radiation from an (electric) point-dipole source, or an assembly of such sources. It is a straightforward matter to decompose an electric point-dipole field into its relevant evanescent and propagating modes, and

thereby estimate the intensity of the phase conjugated field in each of the $q_\parallel$ components. However, in order to determine the characteristics of the phase conjugated light focus generated by the quantum well one would have to calculate the four-wave mixing also for probe fields with wave vectors not confined to the x-z plane, and to do this our theory must first be generalized to nonplanar phase conjugation.

Within the framework of the present theory, it is possible, however, to study the spatial confinement (focusing) of the phase conjugated field generated by a quantum wire adequately placed above the surface of the quantum well,[55] and let us, therefore, as an example consider the case where the source of the probe field is a (quantum) wire. We imagine that the axis of the wire is placed parallel to the y axis and cuts the x-z-plane in the point $(0,-z_0)$, cf. Fig. 1. Under the assumption that the spatial electron confinement in the wire is perfect (complete) and the wire current density is the same all along the wire at a given time, the harmonic source current density is given by

$$\vec{J}(\vec{r};\omega)=\vec{J}_0(\omega)\,\delta(x)\,\delta(z+z_0), \tag{49}$$

where $\vec{J}_0(\omega)$ is its possibly frequency dependent vectorial amplitude. The spatial distribution of the field from this source is[55]

$$\vec{E}(x,z;\omega)=\frac{1}{(2\pi)^2}\int_{-\infty}^{\infty}\vec{E}(z;\vec{q}_\parallel,\omega)e^{i\vec{q}_\parallel\cdot\vec{x}}\delta(q_{\parallel,y})d^2q_\parallel, \tag{50}$$

where

$$\vec{E}(z;\vec{q}_\parallel,\omega)=-\frac{e^{iq_\perp(z+z_0)}}{2\epsilon_0\omega q_\perp}\begin{bmatrix} q_\perp^2 & 0 & -q_\parallel q_\perp \\ 0 & q^2 & 0 \\ -q_\parallel q_\perp & 0 & q_\parallel^2 \end{bmatrix}\cdot\vec{J}_0(\omega), \tag{51}$$

where as before $q_\parallel^2+q_\perp^2=q^2$. At the phase conjugating mirror, the Fourier components of the wire probe are $\vec{E}(-d;\vec{q}_\parallel,\omega)$.

To illustrate the angular spectral distribution of the field from this kind of wire source at the phase conjugator, we look more closely at the cases where the current density is polarized (i) along the x axis and (ii) along the y axis. Thus, in case (i) we use $\vec{J}_0(\omega)=J_0(\omega)\vec{e}_x$, and by normalizing the electric fields to the amplitude of the current density, the corresponding normalized differential intensity $[\Delta I_{\text{probe}} \equiv \frac{1}{2}\epsilon_0 c_0\vec{E}(-d;\vec{q}_\parallel,\omega)\cdot\vec{E}^*(-d,\vec{q}_\parallel,\omega)(2\pi)^{-4}]$,

$$\frac{\Delta I_{\text{probe}}(-d;\vec{q}_\parallel)}{|J_0(\omega)|^2}=\frac{1}{2^7\pi^4\epsilon_0 c_0}\{\Theta(1-(q_\parallel/q))+\Theta((q_\parallel/q)-1)[2(q_\parallel/q)^2-1]\exp[-2(z_0-d)q\sqrt{(q_\parallel/q)^2-1}]\} \tag{52}$$

is shown in Fig. 7 for different values of the distance z_0-d from the wire to the vacuum/film interface. In case (ii), $\vec{J}_0(\omega)=J_0(\omega)\vec{e}_y$, and the associated normalized intensity, which is given by

$$\frac{\Delta I_{\text{probe}}(-d;\vec{q}_\parallel)}{|J_0(\omega)|^2}=\frac{1}{2^7\pi^4\epsilon_0 c_0}\left\{\frac{\Theta(1-(q_\parallel/q))}{1-(q_\parallel/q)^2}+\frac{\Theta((q_\parallel/q)-1)}{(q_\parallel/q)^2-1}\exp[-2(z_0-d)q\sqrt{(q_\parallel/q)^2-1}]\right\}, \tag{53}$$

is also presented in Fig. 7, for the same distances as in case (i). The third curve in Fig. 7 represents the case where $\vec{J}_0(\omega)=J_0(\omega)\vec{e}_z$, and is shown for reference.

Looking at the curve in Fig. 7 corresponding to $\vec{J}_0(\omega)=J_0(\omega)\vec{e}_y$ [and the curve corresponding to $\vec{J}_0(\omega)=J_0(\omega)\vec{e}_z$], we notice that a singularity occurs when $q_\parallel/q=1$, or equivalently where $q_\perp=0$. The presence of this singularity is an artifact originating in the (model) assumption that the electron confinement is complete in the x and z directions [see Eq. (49)]. If we had started from a quantum wire current density of finite (but small) extension in x and z the singularity would have been replaced by a (narrow) peak of finite height. Not only in quantum wire optics, but also in optical studies of quantum dots and wells singularities would appear if complete electron confinement was assumed (in three dimensions and one dimension, respectively). In the present context the assumption of perfect electron confinement works well because we only consider the generated field outside the self-field region of the wire (see, e.g., Ref. 43). In an experiment one would always end up integrating over some finite interval of $q_\parallel$ around the singularity, and this integral can in all cases be proven finite. At each distance of the wire from the phase conjugator the two curves $J_0\vec{e}_x$ and $J_0\vec{e}_z$ in Fig. 7 becomes identical when $(q_\parallel/q)^2\gg 1$, since from Eq. (51) we may derive the relation $E_z=-(q_\parallel/q_\perp)E_x$, and since $q_\parallel/q_\perp\simeq 1$ when $(q_\parallel/q)^2\gg 1$.

When the current oscillates in the direction of the wire, it appears that the field intensity in the evanescent probe modes is very small. An appreciable amount of the radiated energy is stored in components in the region $q_\parallel/q\sim 1$ (and in the propagating modes). To study the phase conjugation of evanescent modes it is therefore better to start from $\vec{J}_0(\omega)=J_0(\omega)\vec{e}_x$ or from $\vec{J}_0(\omega)=J_0(\omega)\vec{e}_z$ because these two probe current densities give rise to significant probe intensities in the evanescent regime. If we look at the curve in Fig. 7 representing the field at the surface of the phase conjugator when the probe is placed at $z_0-d=\lambda/256$, ΔI_{probe} peaks in both these cases at $q_\parallel/q\sim 50$ in the evanescent regime. When the current density oscillates along the surface (in the x direction) there is no singularity (and no peak) at $q_\parallel/q\sim 1$, and the maximum value of I_{probe}, occuring at $q_\parallel/q\sim 50$, is three orders of magnitude larger than the probe intensities of every

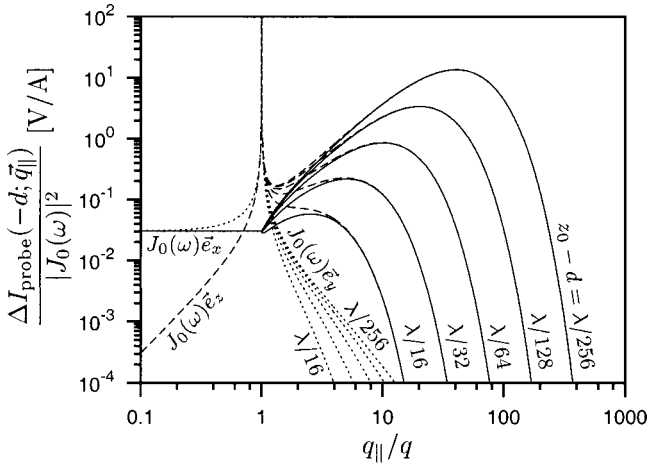

FIG. 7. The angular Fourier spectrum reaching the surface of the phase conjugating medium when the probe field is radiated from a (quantum) wire. The dotted curves $[J_0(\omega)\vec{e}_y]$ show the Fourier components when the wire current density is polarized along the y axis. Similarly, the dashed curves $[J_0(\omega)\vec{e}_z]$ and the fully drawn curves $[J_0(\omega)\vec{e}_x]$ show the Fourier components from a wire source with its current density oscillating along the z axis and the x axis, respectively. The angular Fourier spectrum is for all three cases shown for five different distances $z_0-d\in\{\lambda/16,\ \lambda/32,\ \lambda/64,\ \lambda/128,\ \lambda/256\}$ of the wire from the phase conjugator.

one of the propagating modes. Above $q_\parallel/q\approx 50$ the amplitude of the $q_\parallel$ components descends rapidly and has lost six orders of magnitude within the next order of magnitude of $q_\parallel/q$. At larger probe to surface distances the maximum in the $q_\parallel/q$ spectrum of the probe field at the vacuum/film interface is shifted downwards, and the magnitude becomes smaller, too. That is, compared to the raw p to p reflection coefficient, the intensity of each of the Fourier components available from the probe field begin their own falloff about one to two orders of magnitude before the reflection coefficient descends, depending on the distance from the probe to the surface of the phase conjugator. The s-polarized probe field starts the descending tendency already where the character of the Fourier components shifts from being propagating to evanescent ($q_\perp$ becoming imaginary), cf. the remarks above.

Using a quantum wire as the source for the probe field, the angular spectrum of the phase conjugated response, normalized to the pump fields and the absolute square of the amplitude of the wire current density, is given by

$$R_{\mathrm{PC}}(z;\vec{q}_\parallel)\frac{I_{\mathrm{probe}}(-d;\vec{q}_\parallel)}{|J_0(\omega)|^2}=\frac{I_{\mathrm{PC}}(z;\vec{q}_\parallel)}{I^{(1)}I^{(2)}|J_0(\omega)|^2},\qquad(54)$$

and is obtained numerically by multiplying the energy reflection coefficient, $R_{\mathrm{PC}}(z;\vec{q}_\parallel)$, with the normalized probe intensity, $I_{\mathrm{probe}}(-d;\vec{q}_\parallel)/|J_0(\omega)|^2$. In Fig. 8, the angular spectrum at the vacuum/quantum-well interface ($z=-d$) given by Eq. (54) is shown for the cases where $\vec{J}_0(\omega)=J_0(\omega)\vec{e}_x$ and $\vec{J}_0(\omega)=J_0(\omega)\vec{e}_y$. In both cases data are presented for the wire placed at different distances from the vacuum/film interface. By comparison with the raw reflection data in Fig. 3 it appears that the high end of the reflected $q_\parallel$ spectrum is strongly damped. For the s to p transition we see that the

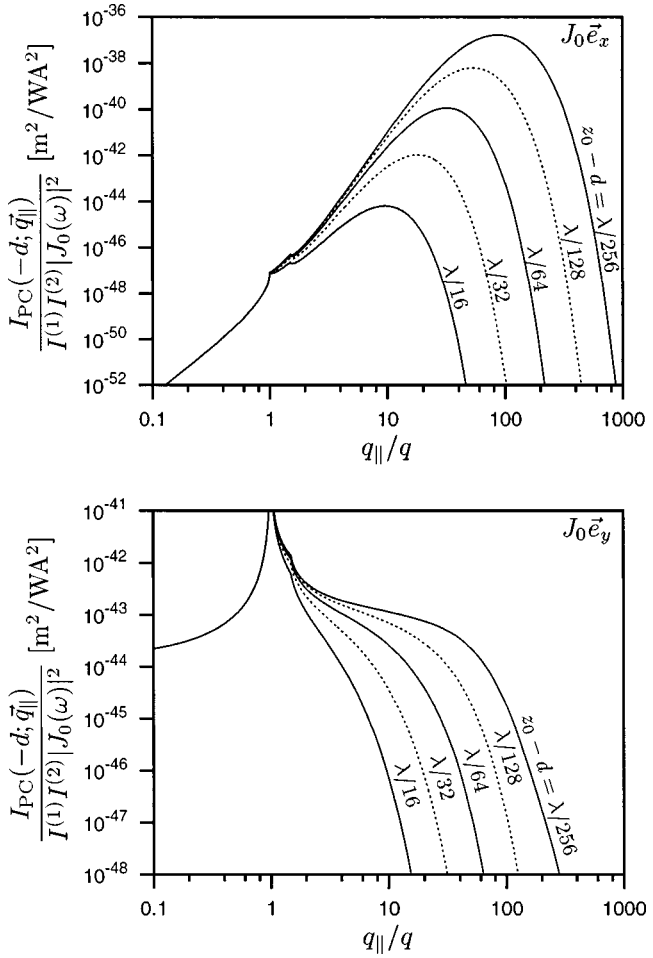

FIG. 8. The convolution of the probe field from a wire source with the phase conjugation reflection coefficient at the vacuum/film interface is shown for different distances between the wire source and the vacuum/film interface, namely, $z_0-d\in\{\lambda/16,\ \lambda/32,\ \lambda/64,\ \lambda/128,\ \lambda/256\}$ as a function of the normalized probe wavenumber $q_\parallel/q$. In the top figure the current density of the wire oscillates along the x axis, and in the bottom figure along the y axis.

energy of the phase conjugated signal is concentrated around $q_\parallel/q=1$, which is mainly due to the fact that the concentration of the radiated energy spectrum from the wire lies around that same point. In the p to p transition we observe that the evanescent components are still by far dominating the response at the place of the wire compared to the propagating components.

IV. CONCLUSIONS

It is evident from our analysis that the phase conjugated response depends strongly on $q_\parallel$, at least for a quantum-well phase conjugator. The nonlinear coupling is strongest in the evanescent part of the spectrum above the point up to which the probe field is propagating in the substrate ($q_\parallel/q=n$). As a consequence, if one wants to observe the phase conjugation of a broad Fourier spectrum of evanescent modes, both observation and excitation near the surface of the phase conjugator is required. The quantum wire offers one possibility of exciting the higher Fourier components, and the phase conjugated response in this case contains a broad range of eva-

nescent components. Because of this the use of a quantum wire source field might be a good candidate for investigating the problem of focusing light beyond the Abbe-Rayleigh[56,57] diffraction limit.

ACKNOWLEDGMENT

The authors would like to acknowledge Dr. H. F. Arnoldus, Department of Physics & Astronomy, Mississippi State University, for fruitful discussions related to this work.

APPENDIX: ANALYTICAL EXPRESSIONS FOR $\mathcal{C}$, $\mathcal{D}$, AND $\mathcal{N}$

In this appendix we discuss how analytic solutions for the integrals over $\vec{\kappa}_\parallel$ appearing in the quantities $\mathcal{C}(q_\parallel - k_\parallel)$, $\mathcal{D}(q_\parallel,k_\parallel)$, and $\mathcal{N}$ may be obtained in the low-temperature limit. Every integral appearing in these quantities can be expressed in the form

$$\mathcal{F}_p^\beta = \int\int \frac{\kappa_y^p f_n(\vec{\kappa}_\parallel + s\vec{e}_x)}{\prod_{k=1}^{\beta}[a_k\kappa_x + b_k]} d\kappa_x d\kappa_y, \tag{A1}$$

where k and β are nonnegative integers, p is an even nonnegative integer, and $s \equiv s(\vec{q}_\parallel,\vec{k}_\parallel)$ is a function of the pump and probe wave vectors. In Eq. (A1) the nominator is a real quantity and the denominator is a complex quantity.

In the low-temperature limit the distribution function is zero outside the Fermi sphere (and equal to one inside) and it is therefore advantageous to shift κ_x by $-s$, and thereafter perform a one-to-one mapping of the x-y plane into polar coordinates (r-θ plane). Using $\kappa_x = r\cos\theta$ and $\kappa_y = r\sin\theta$ the integral in Eq. (A1) is turned into

$$\mathcal{F}_p^\beta = \int_0^\alpha \int_0^{2\pi} \frac{r(r\sin\theta)^p}{\prod_{k=1}^{\beta}[a_k(r\cos\theta - s) + b_k]} d\theta dr. \tag{A2}$$

The quantity $\alpha = \sqrt{k_F^2 - (\pi/d)^2}$ is the radius of the (two-dimensional) Fermi circle. In the quantity $\mathcal{C}(q_\parallel - k_\parallel)$, $\beta = 1$ in the above equation and $p = 0$, and in the quantity $\mathcal{D}(q_\parallel,k_\parallel)$, $\beta = p = 2$. In the quantity $\mathcal{N}$, $p = a_k = 0$ and $b_k = 1$, and the integral can therefore be solved immediately, with the result

$$\mathcal{N} = \frac{4}{(2\pi)^2}\int_0^\alpha \int_0^\pi r\, d\theta dr = \frac{\alpha^2}{2\pi}. \tag{A3}$$

The complexity of the problem can be reduced, since it is possible to express the function with $\beta = 2$ in terms of two functions with $\beta = 1$, namely,

$$\mathcal{F}_p^2(a_1,a_2,b_1,b_2,s) = \frac{a_1\mathcal{F}_p^1(a_1,b_1,s) - a_2\mathcal{F}_p^1(a_2,b_2,s)}{a_1 b_2 - a_2 b_1}. \tag{A4}$$

As a consequence of Eq. (A4), the integrals appearing in $\mathcal{C}$ and $\mathcal{D}$ can now in general be written in terms of functions of the type

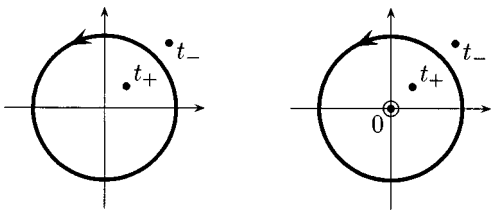

FIG. 9. The poles in the complex t plane in the angular integral of Eq. (A10) are of order 1 at $t_\pm$, as shown to the left. For the angular integral in Eq. (A11) the poles are of order 1 at $t_\pm$ and of order 2 at $t = 0$ as shown to the right. The closed contour shown in each diagram is the integration path used.

$$\mathcal{F}_p^1(a,b,s) = \int_0^\alpha \int_0^{2\pi} \frac{r(r\sin\theta)^p}{b - as + ar\cos\theta} d\theta dr, \tag{A5}$$

where $p \in \{0,2\}$, dropping the now superfluous index on a and b. To solve Eq. (A5), let us make the substitutions

$$\eta \equiv \frac{b - as}{a\alpha}, \quad r \equiv \alpha u, \tag{A6}$$

which turn Eq. (A5) into

$$\mathcal{F}_0^1(\eta) = \frac{\alpha}{a}\int_0^1 \int_0^{2\pi} \frac{u}{\eta + u\cos\theta} d\theta du, \tag{A7}$$

$$\mathcal{F}_2^1(\eta) = \frac{\alpha^3}{a}\int_0^1 \int_0^{2\pi} \frac{u^3\sin^2\theta}{\eta + u\cos\theta} d\theta du. \tag{A8}$$

Next, to carry out the angular integrals, we set

$$t = e^{i\theta} \tag{A9}$$

so that these integrals become

$$\int_0^{2\pi} \frac{1}{\eta + u\cos\theta} d\theta = \frac{1}{iu}\oint \frac{1}{(t - t_+)(t - t_-)} dt, \tag{A10}$$

$$\int_0^{2\pi} \frac{\sin^2\theta}{\eta + u\cos\theta} d\theta = \frac{i}{4u}\oint \frac{(1 - t^2)^2}{t^2(t - t_+)(t - t_-)} dt, \tag{A11}$$

where the poles at $t_\pm$ in the t plane are located at

$$t_\pm = -\frac{\eta}{u} \pm \sqrt{\left(\frac{\eta}{u}\right)^2 - 1}, \tag{A12}$$

and the integration runs along the unit circle. Since we have $t_+ t_- = 1$, one of these poles is inside the unit circle while the other is outside. Using the unit circles shown in Fig. 9 as the integration paths, we find by a residue calculation

$$\int_0^{2\pi} \frac{1}{\eta + u\cos\theta} d\theta = \frac{2\pi}{\sqrt{\eta^2 - u^2}}, \tag{A13}$$

$$\int_0^{2\pi} \frac{\sin^2\theta}{\eta + u\cos\theta} d\theta = \frac{2\pi}{u^2}[\eta - \sqrt{\eta^2 - u^2}]. \tag{A14}$$

By insertion of these results into Eqs. (A7) and (A8) and carrying out the elementary radial integrations one obtains

$$\mathcal{F}_0^1(a,b,s)=\frac{2\pi}{a^2}[b-as-\sqrt{(b-as)^2-a^2\alpha^2}], \tag{A15}$$

$$\mathcal{F}_2^1(a,b,s)=\frac{2\pi}{3a^4}\{[(b-as)^2-\alpha^2a^2]^{3/2}-(b-as)^3 + \tfrac{3}{2}\alpha^2a^2(b-as)\}. \tag{A16}$$

Finally, the quantities $\mathcal{C}(q_\parallel \pm k_\parallel)$ and $\mathcal{D}(q_\parallel,k_\parallel)$ can be expressed as

$$\mathcal{C}(q_\parallel \pm k_\parallel)=2[\mathcal{F}_0^1(a_1,b_1,q_\parallel \pm k_\parallel)-\mathcal{F}_0^1(a_1,b_1,0)], \tag{A17}$$

and

$$\begin{aligned}\mathcal{D}(q_\parallel,k_\parallel)=2[&\mathcal{F}_2^2(a_2,a_3,b_2,b_3,0)-\mathcal{F}_2^2(a_2,a_3,b_2,b_3,k_\parallel)\\ &+\mathcal{F}_2^2(a_2,a_4,b_2,b_4,k_\parallel+q_\parallel)\\ &-\mathcal{F}_2^2(a_2,a_4,b_2,b_4,k_\parallel)+\mathcal{F}_2^2(a_2,a_4,b_2,b_5,0)\\ &-\mathcal{F}_2^2(a_2,a_4,b_2,b_5,q_\parallel)\\ &+\mathcal{F}_2^2(a_2,a_3,b_2,b_6,k_\parallel+q_\parallel)\\ &-\mathcal{F}_2^2(a_2,a_3,b_2,b_6,q_\parallel)],\end{aligned} \tag{A18}$$

where

$$a_1=\hbar(q_\parallel-k_\parallel)/m_e, \tag{A19}$$

$$a_2=\hbar(q_\parallel+k_\parallel)/m_e, \tag{A20}$$

$$a_3=\hbar k_\parallel/m_e, \tag{A21}$$

$$a_4=\hbar q_\parallel/m_e, \tag{A22}$$

$$b_1=\hbar(q_\parallel-k_\parallel)^2/(2m_e)-i/\tau, \tag{A23}$$

$$b_2=\hbar(q_\parallel+k_\parallel)^2/(2m_e)-i/\tau, \tag{A24}$$

$$b_3=\hbar k_\parallel^2/(2m_e)-i/\tau-\omega, \tag{A25}$$

$$b_4=\hbar q_\parallel(q_\parallel+2k_\parallel)/(2m_e)-i/\tau+\omega, \tag{A26}$$

$$b_5=\hbar q_\parallel^2/(2m_e)-i/\tau+\omega, \tag{A27}$$

$$b_6=\hbar k_\parallel(k_\parallel+2q_\parallel)/(2m_e)-i/\tau-\omega. \tag{A28}$$

[1] J. E. Sipe and G. I. Stegeman, in *Surface Polaritons*, edited by V. M. Agranovich and D. L. Mills (North-Holland, Amsterdam, 1982).

[2] G. L. Richmond, J. M. Robinson, and V. L. Shannon, Prog. Surf. Sci. **28**, 1 (1988).

[3] T. F. Heinz, in *Nonlinear Surface Electromagnetic Phenomena*, edited by H.-E. Ponath and G. I. Stegeman (Elsevier, Amsterdam, 1991), pp. 353–416.

[4] G. A. Reider and T. F. Heinz, in *Photonic Probes of Surfaces*, edited by P. Halevi (North-Holland, Amsterdam, 1995), pp. 413–478.

[5] A. Liebsch, in *Photonic Probes of Surfaces*, edited by P. Halevi (North-Holland, Amsterdam, 1995), pp. 479–532.

[6] K. Pedersen, in *Studies in Classical and Quantum Nonlinear Phenomena*, edited by O. Keller (Nova Science, New York, 1995), pp. 385–418.

[7] R. Bavli and Y. B. Band, Phys. Rev. A **43**, 5044 (1991).

[8] O. Keller, Phys. Rev. B **48**, 4786 (1993).

[9] F. T. Vasko, Phys. Rev. B **53**, 9576 (1996).

[10] X. Chen and O. Keller, Phys. Rev. B **55**, 15 706 (1997).

[11] O. Keller and G. Wang, Phys. Rev. B **56**, 12 327 (1997).

[12] O. A. Aktsipetrov, A. V. Melnikov, T. V. Murzina, A. A. Nikulin, and A. N. Rubtsov, Surf. Sci. **336**, 225 (1995).

[13] O. A. Aktsipetrov, A. A. Fedyanin, and M. C. Downer, in *Notions and Perspectives of Nonlinear Optics*, edited by O. Keller (World Scientific, Singapore, 1996), pp. 301–338.

[14] U. Pustogowa, W. Hubner, and K. H. Bennemann, Surf. Sci. **307–309**, A1129 (1994).

[15] A. Liu and O. Keller, Phys. Scr. **52**, 116 (1995).

[16] T. Rasing and M. G. Goerkamp, Proc. SPIE **2801**, 96 (1995).

[17] T. Rasing, in *Notions and Perspectives of Nonlinear Optics*, edited by O. Keller (World Scientific, Singapore, 1996), pp. 339–369.

[18] J. S. Nkoma, J. Phys.: Condens. Matter **1**, 9623 (1989).

[19] E. Z. Mishchenko and L. A. Fal'kovskii, JETP **80**, 531 (1995).

[20] F. J. Garcia-Vidal and J. B. Pendry, Phys. Rev. Lett. **77**, 1163 (1996).

[21] R. Haight, Surf. Sci. Rep. **21**, 275 (1995).

[22] T. Fauster and W. Steinmann, in *Photonic Probes of Surfaces*, edited by P. Halevi (North-Holland, Amsterdam, 1995), pp. 347–411.

[23] A. T. Georges, Phys. Rev. B **51**, 13 735 (1995).

[24] V. M. Shalaev, C. Douketis, T. Haslett, T. Stuckless, and M. Moskovits, Phys. Rev. B **53**, 11 193 (1996).

[25] Y. S. Tergiman, K. Warda, C. Girardeau-Montaut, and J.-P. Girardeau-Montaut, Opt. Commun. **142**, 126 (1997).

[26] D. von der Linde, in *Notions and Perspectives of Nonlinear Optics*, edited by O. Keller (World Scientific, Singapore, 1996), pp. 234–271.

[27] *Atoms in Intense Fields*, edited by M. Garvila (Academic Press, Boston, 1992).

[28] *Optical Phase Conjugation*, edited by R. A. Fisher (Academic Press, New York, 1983).

[29] B. Y. Zel'dovich, N. F. Pilipetsky, and V. V. Shkunov, *Principles of Phase Conjugation* (Springer-Verlag, Berlin, 1985).

[30] D. M. Pepper, in *Laser Handbook, Volume 4*, edited by M. L. Stitch and M. Bass (North-Holland, Amsterdam, 1985), pp. 333–485.

[31] J.-I. Sakai, *Phase Conjugate Optics* (McGraw-Hill, New York, 1992).

[32] *Optical Phase Conjugation*, edited by M. Gower and D. Proch (Springer-Verlag, Berlin, 1994).

[33] M. Fukui, J. E. Sipe, V. C. Y. So, and G. I. Stegeman, Solid State Commun. **27**, 1265 (1978).

[34] K. Ujihara, Opt. Commun. **42**, 1 (1982).

[35] K. Ujihara, Opt. Commun. **43**, 225 (1982).

[36] K. Ujihara, J. Opt. Soc. Am. **73**, 610 (1983).
[37] B. H. W. Hendriks and G. Nienhuis, Phys. Rev. A **40**, 1892 (1989).
[38] G. S. Agarwal and S. D. Gupta, Opt. Commun. **119**, 591 (1995).
[39] O. Keller, J. Nonlinear Opt. Phys. Mater. **5**, 109 (1996).
[40] H. F. Arnoldus and T. F. George, Phys. Rev. A **51**, 4250 (1995).
[41] T. Andersen and O. Keller, Phys. Scr. (to be published).
[42] O. Keller, Phys. Rep. **268**, 85 (1996).
[43] O. Keller, in *Progress in Optics XXXVII*, edited by E. Wolf (Elsevier, Amsterdam, 1997), pp. 257–343.
[44] P. J. Feibelman, Prog. Surf. Sci. **12**, 287 (1982).
[45] S. I. Bozhevolnyi, O. Keller, and I. I. Smolyaninov, Opt. Lett. **19**, 1601 (1994).
[46] N. W. Ashcroft and N. D. Mermin, *Solid State Physics* (Holt, Rinehart and Winston, New York, 1976).
[47] M. Jalochowski, M. Stróżak, and R. Zdyb (unpublished).
[48] A. Yariv, Opt. Commun. **40**, 401 (1982).
[49] A. Otto, Z. Phys. **216**, 398 (1968).
[50] A. Otto, in *Optical Properties of Solids New Developments*, edited by B. O. Seraphin (North-Holland, Amsterdam, 1976), pp. 677–729.
[51] E. Kretschmann and H. Raether, Z. Naturforsch. A **23**, 2135 (1968).
[52] H. Raether, *Surface Plasmons on Smooth and Rough Surfaces and Gratings* (Springer-Verlag, Berlin, 1988).
[53] *Near Field Optics*, edited by D. W. Pohl and D. Courjon (Kluwer, Dordrecht, 1993).
[54] *Optics at the Nanometer Scale*, edited by M. Nieto-Vesperinas and N. García (Kluwer, Dordrecht, 1996).
[55] O. Keller, in *Computational Studies of New Materials*, edited by D. A. Jelski and T. F. George (World Scientific, Singapore, 1998).
[56] E. Abbe, Arch. Mikrosk. Anat. **9**, 413 (1873).
[57] Lord Rayleigh, Philos. Mag. **42**, 167 (1896).